THE JOURNAL OF BIOLOGICAL CHEMISTRY VOL. 291, NO. 12, pp. 6456–6470, March 18, 2016
© 2016 by The American Society for Biochemistry and Molecular Biology, Inc. Published in the U.S.A.

Modulation of DNA Polymerase Noncovalent Kinetic Transitions by Divalent Cations*

Received for publication, November 2, 2015, and in revised form, January 2, 2016 Published, JBC Papers in Press, January 21, 2016, DOI 10.1074/jbc.M115.701797

Joseph M. Dahl[‡1], **Kate R. Lieberman**[‡2], **and Hongyun Wang**[§3]

From the Departments of [‡]*Biomolecular Engineering and* [§]*Applied Mathematics and Statistics, University of California, Santa Cruz, California 95064*

Replicative DNA polymerases (DNAPs) require divalent metal cations for phosphodiester bond formation in the polymerase site and for hydrolytic editing in the exonuclease site. Me^{2+} ions are intimate architectural components of each active site, where they are coordinated by a conserved set of amino acids and functional groups of the reaction substrates. Therefore Me^{2+} ions can influence the noncovalent transitions that occur during each nucleotide addition cycle. Using a nanopore, transitions in individual Φ29 DNAP complexes are resolved with single-nucleotide spatial precision and sub-millisecond temporal resolution. We studied Mg^{2+} and Mn^{2+}, which support catalysis, and Ca^{2+}, which supports deoxynucleoside triphosphate (dNTP) binding but not catalysis. We examined their effects on translocation, dNTP binding, and primer strand transfer between the polymerase and exonuclease sites. All three metals cause a concentration-dependent shift in the translocation equilibrium, predominantly by decreasing the forward translocation rate. Me^{2+} also promotes an increase in the backward translocation rate that is dependent upon the primer terminal 3′-OH group. Me^{2+} modulates the translocation rates but not their response to force, suggesting that Me^{2+} does not affect the distance to the transition state of translocation. Absent Me^{2+}, the primer strand transfer pathway between the polymerase and exonuclease sites displays additional kinetic states not observed at >1 mM Me^{2+}. Complementary dNTP binding is affected by Me^{2+} identity, with Ca^{2+} affording the highest affinity, followed by Mn^{2+}, and then Mg^{2+}. Both Ca^{2+} and Mn^{2+} substantially decrease the dNTP dissociation rate relative to Mg^{2+}, while Ca^{2+} also increases the dNTP association rate.

DNA polymerases (DNAPs)[4] are responsible for accurate replication of DNA genomes. Replicative DNAPs achieve this by catalyzing template-directed polymerization of deoxyribonucleoside triphosphates (dNTPs) with extremely high fidelity (with error rates of $\sim 10^{-6}$ to $\sim 10^{-8}$) (1, 2). Phosphodiester bond formation, the chemical transformation during polymerization, is catalyzed in the polymerase active site, in the 5′ to 3′ direction. Many replicative DNAPs also catalyze a second nucleotidyl transfer reaction, the exonucleolytic cleavage of the primer strand in the 3′ to 5′ direction. This editing reaction allows for removal of incorrect nucleotides inserted during polymerization, contributing ~1–2 orders of magnitude to replication fidelity (1). Exonucleolytic editing occurs in a separate active site that is typically ~30–40 Å from the polymerase site (3–9), and it requires that ~3 base pairs of the nascent primer-template duplex be melted to allow the primer strand to be transferred from the polymerase site to the exonuclease site.

An essential role for two divalent metal cations (Me^{2+} ions) in the mechanism of numerous enzyme-catalyzed nucleotidyl transfer reactions has been characterized (10), in which one Me^{2+} ion (termed metal A) serves primarily to activate the nucleophile, whereas the other (termed metal B) mitigates the negative charge that builds in the transition state (10, 11). For replicative DNAPs, this two Me^{2+} ion mechanism applies to both phosphodiester bond formation in the polymerase site, and to hydrolysis of the primer terminal dNMP residue in the exonuclease site (12, 13). In accord with their roles in the chemical transformations, the Me^{2+} ions are intimate architectural components of each of the active sites. They are coordinated by a highly conserved set of acidic amino acid side chains in each site, as well as by specific functional groups of the reaction substrates. Therefore, in addition to their essential role in the chemical reactions, Me^{2+} ions may also influence the reversible noncovalent transitions that govern the fate of DNAP-DNA complexes after each covalent nucleotide addition. These transitions include (i) the primer strand transfer between the polymerase and exonuclease sites, (ii) the translocation fluctuations, in which the DNA substrate moves between the pre-translocation and post-translocation states in the DNAP polymerase site, a spatial displacement of the distance of a single nucleotide, and (iii) dNTP binding in the polymerase site. In contrast to the roles of the Me^{2+} ions in the chemical steps of dNTP polymerization and exonucleolysis, much less is known about the effects of Me^{2+} ions on these noncovalent transitions in DNAP complexes.

The conserved architecture of the DNAP domain that contains the polymerase active site resembles a partially closed hand, comprising palm, thumb, and fingers subdomains (3, 4, 9, 14, 15). The palm subdomain contains residues that participate in catalysis of phosphodiester bond formation, including the acidic residues involved in Me^{2+} coordination. The fingers subdomain contains residues essential for binding incoming nucle-

* This work was supported, in whole or in part, by National Institutes of Health Grant R01GM087484 from NIGMS (to K. R. L.). The authors declare that they have no conflicts of interest with the contents of this article. The content is solely the responsibility of the authors and does not necessarily represent the official views of the National Institutes of Health.

[1] Supported by an National Science Foundation Graduate Research Fellowship DGE 1339067.

[2] To whom correspondence may be addressed: Baskin School of Engineering, 1156 High St., Santa Cruz, CA 95064. E-mail: krlieberman@gmail.com.

[3] To whom correspondence may be addressed. E-mail: hongwang@soe.ucsc.edu.

[4] The abbreviation used is: DNAP, DNA polymerase.

This is an Open Access article under the CC BY license.

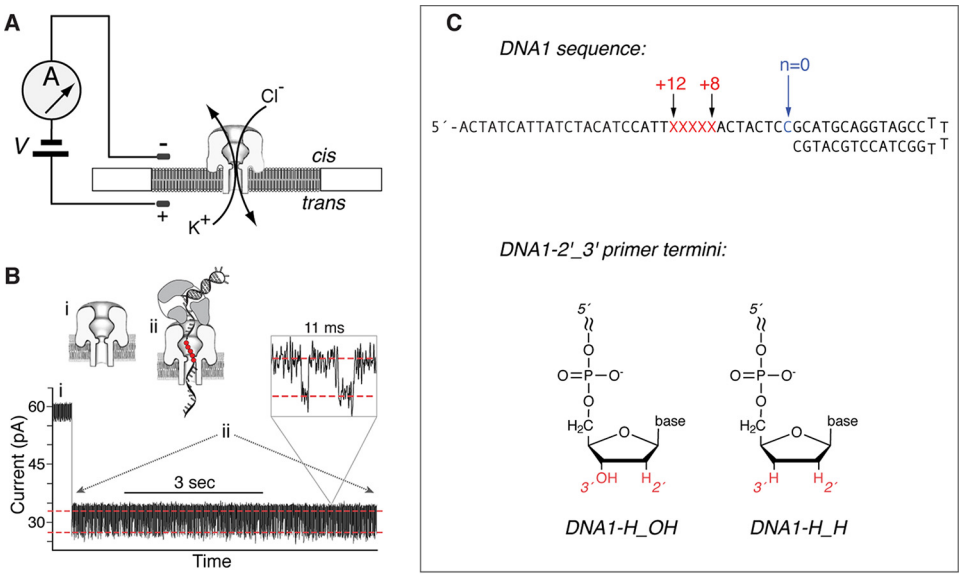

FIGURE 1. **Capture of individual DNAP complexes.** *A*, a single α-hemolysin nanopore is inserted in a ~25-μm diameter lipid bilayer separating two chambers (*cis* and *trans*) containing buffer solution. A patch clamp amplifier applies voltage across the bilayer and measures ionic current carried through the pore by K^+ and Cl^- ions. *B*, ionic current time trace for a binary complex formed between wild type Φ29 DNAP and a DNA substrate (DNA1-H_H, in *panel C*) captured at 180 mV applied potential in buffer containing 10 mM K-Hepes, pH 8.0, 0.3 M KCl, 1 mM EDTA, 1 mM DTT, and 11 mM $MgCl_2$. Φ29 DNAP and DNA1-H_H were added to the nanopore *cis* chamber to final concentrations of 0.75 and 1 μM, respectively. Schematics *above* the current trace illustrate the sequence of events: (i) the ionic current through the open nanopore; (ii) the current drops rapidly when a complex is captured. The enzyme is too large to enter the nanopore, and therefore the complex, with the enzyme bound at the primer-template junction of the DNA substrate, perches atop the pore. The DNA template strand of the complex is suspended through the nanopore lumen, which is just wide enough to accommodate a single strand of DNA. Individual complexes reside atop the nanopore for tens of seconds, during which the measured ionic current fluctuates on the millisecond time scale between two amplitude levels (*inset*). Transition between the two amplitudes corresponds to movement of the DNA substrate relative to the enzyme and the nanopore by the distance of a single nucleotide (23, 35, 39). This spatial displacement of the DNA substrate that occurs during the translocation is detected in the time traces of ionic current by the use of a reporter group of five consecutive abasic (1′-H, 2′-H) residues in the template strand (*red circles* in the schematic). The fluctuations between the two amplitudes continue until complexes dissociate or are ejected, after which another complex can be captured. *C*, DNA hairpin substrates comprise a 14-base pair duplex region and a single-stranded template region of 35 nucleotides. The reporter group of five abasic (1′, 2′-H) residues spans positions +8 to +12 (*red Xs* in the sequence). DNA1-H_OH bears a 2′-H, 3′-OH primer terminus and DNA1-H_H bears a 2′-H, 3′-H primer terminus.

otide substrates. When dNTP binds to the polymerase active site in the post-translocation state, elements of the fingers subdomain move relative to their position in complexes lacking dNTP, closing in toward the active site to achieve a tight steric fit for the nascent base pair. In the fingers-closed dNTP-bound complex, the 3′-OH group of the DNA primer strand and a non-bridging oxygen of the α phosphate are ligands for one of the Me^{2+} ions (metal A) and non-bridging oxygens of all three phosphate groups are ligands for the metal B ion (4, 15–17).

A hypothesis for the structural basis of translocation in the B family of replicative DNAPs has been proposed (3). The B family includes pol ϵ and pol δ, the enzymes that catalyze leading and lagging strand genomic replication, respectively, in eukaryotes (18, 19). Core structure, catalytic mechanisms, and functional properties are highly conserved in this DNAP family (2, 3, 8, 9, 20, 21). Based upon the comparison of crystal structures of the DNAP from bacteriophage Φ29 in the fingers-open, post-translocation state DNAP-DNA binary complex or in the fingers-closed, post-translocation state DNAP-DNA-dNTP ternary complex (3), it was proposed that the post-translocation state ternary complex can serve as a model for the structure of a fingers-closed, pre-translocation state complex. In this view, the nascent base pair between the templating base at $n = 0$ and the incoming complementary dNTP in the post-translocation state ternary complex occupies the site that would be occupied by the terminal base pair of the primer-template duplex in the pre-translocation state complex. The structure of the binary complex in the fingers-open, post-translocation state indicates that the pre-translocation state in the fingers-open conformation is sterically precluded, and hence fingers opening was proposed to accompany the forward translocation (3). Little is known about whether Me^{2+} ions that interact with complexes in the polymerase active site in the pre-translocation or post-translocation states exert any influence on the translocation fluctuations. For the X-family mammalian repair DNAP, pol β, there is evidence that Me^{2+} can stabilize the pre-translocation state in DNAP-DNA binary complexes (22).

We have developed a single-molecule approach using a nanoscale pore (Fig. 1, *A* and *B*) that permits quantification of the rates of translocation fluctuations, rates of the primer strand transfer between the polymerase and exonuclease sites, and rates of dNTP binding, in individual DNAP-DNA complexes (23–26). We used the B-family replicative Φ29 DNAP, which serves as an excellent model system for leading strand DNA synthesis catalyzed in more complex B family replisomes. It catalyzes highly processive DNA synthesis while remaining tightly associated with its DNA substrate and promoting downstream strand displacement during replication (3, 27–30), obviating the need for accessory proteins such as sliding clamps or helicases. Primer strand transfer between the Φ29 DNAP polymerase and exonuclease sites is an intramolecular process (31).

When a complex formed between Φ29 DNAP and a primer template DNA substrate (Fig. 1*C*) is captured atop an α-hemolysin nanopore in an applied electric field (Fig. 1, *A* and *B*), it

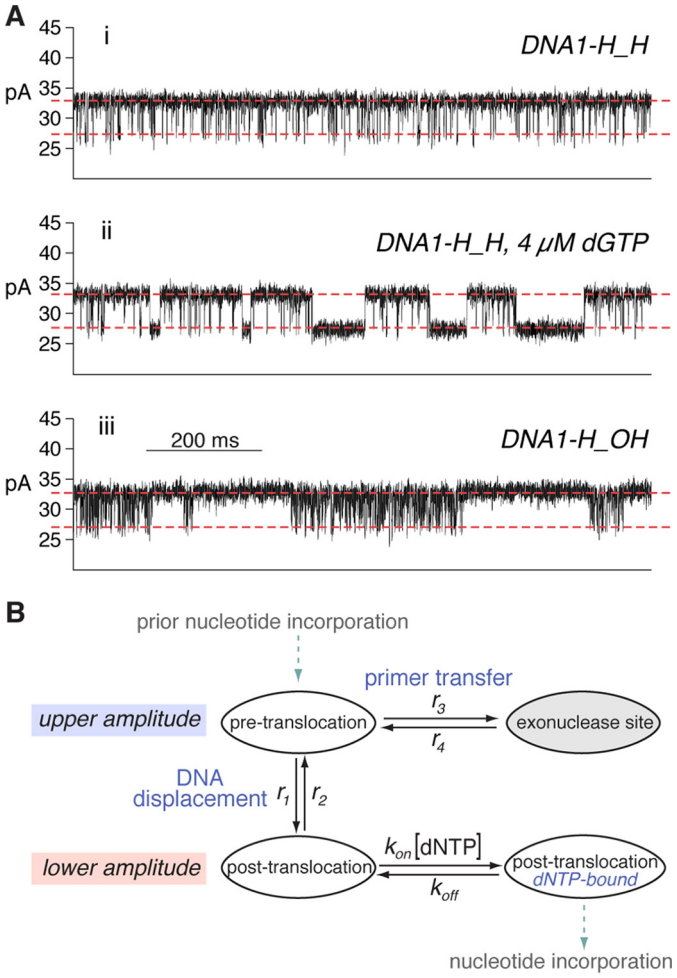

FIGURE 2. **Kinetic transitions resolved in individual Φ29 DNAP complexes captured atop a nanoscale pore.** *A*, ionic current time traces for complexes captured at 180 mV in the presence 10 mM Mg^{2+}. Complexes were formed between the D12A/D66A mutant of Φ29 DNAP and (i) DNA1-H_OH; or (ii) and (iii) DNA1-H_H. In (iii) 4 μM dGTP was present in the *cis* chamber. The *two red dashed lines* indicate the two amplitude levels between which the measured current fluctuates; at 180 mV, the upper amplitude is centered at ~32 pA, and the lower amplitude is centered at ~26 pA at 180 mV. *B*, four-state model for the reversible, noncovalent transitions that govern the fate of replicative DNAP complexes following each covalent nucleotide addition. The model shows the kinetic relationships among the steps of translocation, primer strand transfer between the polymerase and exonuclease active sites, and dNTP binding. Transfer of the primer strand from the polymerase to the exonuclease site precedes the forward translocation (26), and the forward translocation precedes dNTP binding; the translocation is rectified but not driven by dNTP binding, and dNTP has no influence on the rates across the translocation step (25). The kinetic model comprises six transition rates: the rates of translocation (r_1, r_2), the rates of primer stand transfer between the pre-translocation state polymerase site and the exonuclease site (r_3, r_4), and the rates of dNTP binding to post-translocation state complexes (k_{on}[dNTP] and k_{off}). The mathematical framework based on the model allows these rates to be determined from experimental measurements (24–26). Each of the three *unshaded ellipses* corresponds to a state (pre-translocation state, post-translocation state, or dNTP-bound post-translocation state) in which the primer strand, in duplex with the template strand, resides in the polymerase site; the *ellipse* that is *shaded gray* corresponds the state in which the primer terminus resides in the exonuclease site.

undergoes iterative fluctuations across the translocation step. The forward and reverse fluctuations across the translocation step are recorded as discrete transitions between two amplitudes in time traces of ionic current (Figs. 1*B*, *ii*, *inset*, and 2*A*). Each individual captured complex resides atop the nanopore and undergoes the amplitude fluctuations for several seconds, and in each experiment, hundreds of DNAP-DNA complexes can be captured and examined one-by-one, in series. Dwell time samples of each amplitude level are extracted from the ionic current time traces and used to quantify transitions with sub-millisecond temporal resolution and single nucleotide spatial precision.

Complexes formed between Φ29 DNAP and DNA1-H_H captured in the presence of 10 mM Mg^{2+} fluctuate rapidly between the two ionic current amplitudes (Figs. 1*B* and 2*A*, *i*). Addition of dNTP complementary to the templating base at $n = 0$ (dGTP) stabilizes the lower amplitude post-translocation state (Fig. 2*A*, *ii*) (23, 25). In contrast to complexes formed with DNA1-H_H (Fig. 2*A*, *i*), complexes formed with DNA1-H_OH display an additional kinetic state at the upper amplitude. The presence of this state can be directly observed in the time traces as pauses of tens to hundreds of milliseconds that punctuate intervals of rapid fluctuation between the two amplitudes (Fig. 2*A*, *iii*). We showed that the periods of rapid fluctuation are due to transitions between the pre-translocation and post-translocation states and that the pauses in the upper amplitude arise when the primer strand is transferred from the polymerase active site to the exonuclease site (26). Thus, the upper amplitude comprises the pre-translocation state in the polymerase site and the state in which the primer strand occupies the exonuclease site; the lower amplitude comprises the post-translocation state in the polymerase site (23–26).

When an individual DNAP-DNA complex is held atop the nanopore, the applied voltage exerts a force on the complex along the direction of the translocation. This applied force shifts the translocation equilibrium toward the upper amplitude, pre-translocation state (23, 24); it impedes the rate of the forward translocation and increases the rate of the reverse translocation (23, 24), but it does not affect the rates of dNTP binding (25) or the rates of primer strand transfer between the polymerase and exonuclease sites (26). Based on translocation fluctuations measured under varying opposing force loads and in the presence of varying nucleotide concentrations, we established the kinetic relationship of the translocation to the step of nucleotide binding and to the step of primer strand transfer between the polymerase and exonuclease sites (Fig. 2*B*). Specifically, we showed that the forward translocation precedes dNTP binding; the translocation fluctuation is rectified but not driven by dNTP binding, and dNTP has no influence on the rates of the translocation fluctuations (Fig. 2*B*) (25). Furthermore, we established that transfer of the primer strand from the polymerase to the exonuclease site occurs prior to the forward translocation fluctuation; the pre-translocation state is therefore the branch point between the DNA synthesis and editing pathways (Fig. 2*B*) (26). We developed mathematical methods to determine the forward (r_1) and reverse (r_2) rates of translocation fluctuations, the forward (r_3) and reverse (r_4) rates of primer strand transfer between the polymerase and exonuclease sites, and the rates of dNTP or rNTP association (k_{on}) and dissociation (k_{off}) in individual DNAP complexes (Fig. 2*B*) (24–26, 32).

In prior studies (23, 24, 26, 32, 33), we applied these capabilities to examine the kinetic mechanisms by which mutations of highly conserved DNAP residues, alterations in DNA substrate

sequence or structure, or alterations in nucleotide substrate structure exert their influence on DNAP function. The majority of these studies were conducted using complexes captured in the presence of a high concentration of Mg^{2+} (10 mM). In the current study, we have examined the effects of Me^{2+} ions on noncovalent transitions that are essential to DNAP function. We determined the concentration-dependent effects of Mg^{2+}, Mn^{2+}, and Ca^{2+} on the translocation fluctuations, on primer strand transfer between the polymerase and exonuclease sites, and on dNTP binding, in individual Φ29 DNAP-DNA complexes. Mg^{2+} and Mn^{2+} are metals that support catalysis in both the polymerase and exonuclease active sites, whereas Ca^{2+} supports nucleotide binding but not catalysis in either the polymerase or the exonuclease active sites (34).

Experimental Procedures

DNA and Enzymes—DNA substrates were synthesized at Stanford Protein and Nucleic Acid Facility and purified by denaturing PAGE. DNA hairpins were annealed by heating at 90 °C for 4 min followed by snap cooling in ice water. Wild type Φ29 DNAP was obtained from Enzymatics (Beverly, MA). The D12A/D66A mutant was obtained from XPol Biotech (Madrid, Spain).

Nanopore Methods—Nanopore experiments were conducted as described (23, 25, 35–38). A single α-hemolysin nanopore is inserted in a ~25-μm diameter lipid bilayer that separates two chambers (*cis* and *trans*) containing buffer solution (10 mM K-Hepes, pH 8.0, 0.3 M KCl, and 1 mM DTT). DNA and Φ29 DNAP were added to the *cis* chamber to final concentrations of 1 and 0.75 μM, respectively. $MgCl_2$, $CaCl_2$, $MnCl_2$, or EDTA were added to the *cis* well as indicated in the text and figure legends. Ionic current was measured with an integrating patch clamp amplifier (Axopatch 200B, Molecular Devices) in voltage clamp mode. Data were sampled using an analog-to-digital converter (Digidata 1440A, Molecular Devices) at 100 kHz in whole cell configuration and filtered at 5 kHz using a low pass Bessel filter.

Detection of the Translocation in Captured DNAP-DNA Complexes—The displacement of the DNA relative to the enzyme that occurs during translocation is detected with single nucleotide spatial precision and sub-millisecond temporal resolution by the use of a reporter group in the template strand of the DNA substrate, and has been described in detail (23–26, 32, 33, 35, 39). Briefly, the reporter comprises five consecutive abasic (1′,2′-H) residues (shown as *red X*s in the sequence in Fig. 1*C* and as *solid red circles* in the schematic in Fig. 1*B*). When the reporter resides within the pore lumen, the abasic residues allow more ions to flow through the channel than a strand composed of normal DNA residues alone. The extent to which the abasic reporter augments the amplitude of captured complexes depends upon its position relative to the limiting aperture of the nanopore lumen. Thus, displacement of the abasic reporter group in the nanopore lumen is manifested as a change in measured ionic current (23, 35).

Analysis of Ionic Current Time Traces—The extraction of the dwell time samples of the upper and lower amplitudes from recorded time traces of ionic current, and the calculation of kinetic transition rates, has been described in detail (26, 32).

Estimating Free [dNTP] in Bulk Phase—Due to the high affinity of Φ29 DNAP-DNA complexes for dNTP in Mn^{2+} and Ca^{2+} it was necessary to measure complementary dNTP binding by adding very low concentrations of dGTP to the bulk phase in the *cis* well (Fig. 10). In bulk phase, dGTP may bind onto complexes to form ternary complexes. As a result, not all added dGTP molecules are free in bulk. When the added dGTP concentration is lower than the enzyme concentration, the concentration of free dGTP in bulk may be significantly different from that of added dGTP. Therefore, we need to calculate the free dGTP concentration.

Let p = probability of lower amplitude (post-translocation state, with or without dNTP bound); $[dGTP]_0$ = concentration of added dGTP in bulk; $[DNAP{\cdot}DNA]_0$ = concentration of added enzyme-DNA complexes in bulk; $[dGTP]_{Free}$ = concentration of free dGTP in bulk; $K_d^{(bulk)}$ = apparent binding affinity of dGTP onto enzyme-DNA complexes in bulk; and K_d = binding affinity of dGTP onto an enzyme-DNA complex that is captured atop the pore and is in the post-translocation configuration. Note that $K_d^{(bulk)}$ may be different from K_d because in bulk, not all enzyme molecules are necessarily at the primer-template junction, and for complexes with enzyme at the primer-template junction, not all of them are in the post-translocation state (the state competent to bind dNTP) at all times. So, in our model, we allow $K_d^{(bulk)}$ to be different from K_d.

In experiments, $[DNAP{\cdot}DNA]_0$ is fixed at 0.75 μM and $[dGTP]_0$ is a control variable. As a function of $[dGTP]_0$ and $K_d^{(bulk)}$, the concentration of free dGTP in bulk has the following expression.

$$[dGTP]_{Free}([dGTP]_0, K_d^{(bulk)}) = \frac{[dGTP]_0 - [DNAP \cdot DNA]_0 - K_d^{(bulk)}}{2} + \frac{\sqrt{([dGTP]_0 + [DNAP \cdot DNA]_0 + K_d^{(bulk)})^2 - 4[dGTP]_0 \cdot [DNAP \cdot DNA]_0}}{2} \quad \text{(Eq. 1)}$$

Previously (23) we established that the normalized $p/(1-p)$ is related to the free dGTP concentration by Equation 2.

$$\text{Normalized } \frac{p}{1-p} = 1 + \frac{[dGTP]_{Free}}{K_d} \quad \text{(Eq. 2)}$$

It follows that log(normalized $p/(1-p) - 1$) is a linear function of $\log([dGTP]_{Free})$ with slope 1.

$$\text{Log}\left(\text{normalized } \frac{p}{1-p} - 1\right) = \log([dGTP]_{Free}([dGTP]_0, K_d^{(bulk)})) - \log(K_d) \quad \text{(Eq. 3)}$$

In dGTP titration experiments, values of normalized $p/(1-p)$ are observed for a sequence of $[dGTP]_0$ values. For a given value of $K_d^{(bulk)}$, a sequence of $[dGTP]_{Free}$ values are calculated from the $[dGTP]_0$ values. Data points of Equation 4

$$\text{Log}([dGTP]_{Free}) \text{ versus } \log\left(\text{normalized } \frac{p}{1-p} - 1\right) \quad \text{(Eq. 4)}$$

are fitted to a straight line with slope 1. The deviation of data points from the fitting line is used to measure how well data

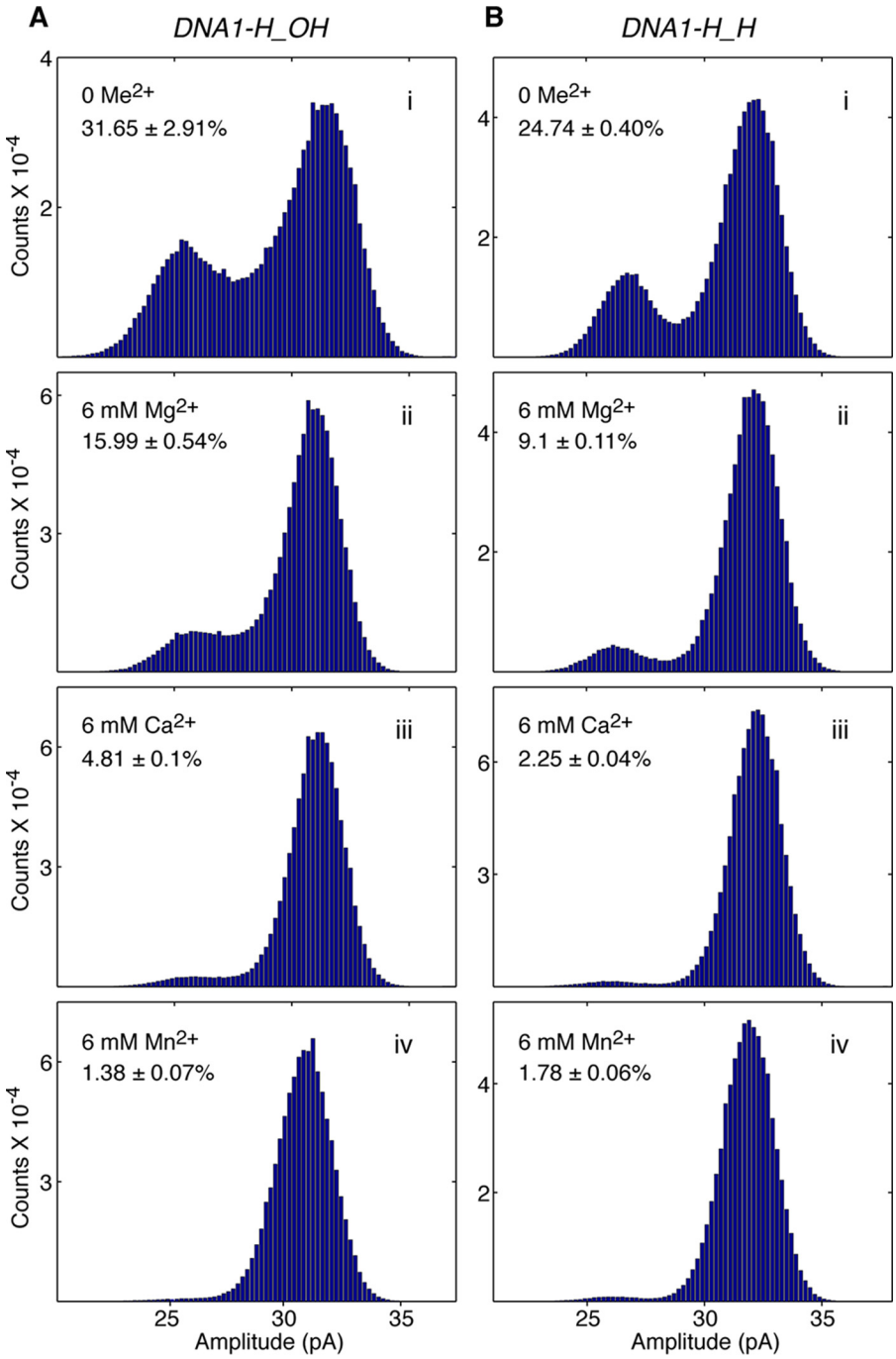

FIGURE 3. **Me^{2+} decreases the probability of the post-translocation state.** Amplitude histograms for complexes formed between the D12A/D66A mutant of Φ29 DNAP and (*A*) DNA1-H_OH or (*B*) DNA1-H_H, captured in the presence of (i) 0 Me^{2+}, (ii) 6 mM Mg^{2+}, (iii) 6 mM Ca^{2+}, or (iv) 6 mM Mn^{2+}.

points follow a straight line with slope 1. The value of $K_d^{(bulk)}$ is determined by minimizing this deviation.

Once the value of $K_d^{(bulk)}$ is calculated, we calculate the free dGTP concentration $[dGTP]_{Free}$ corresponding to each added dGTP concentration $[dGTP]_0$.

Results

When Φ29 DNAP complexes are captured atop the nanopore in the absence of added Me^{2+}, the measured ionic current fluctuates between the two amplitudes that are characteristic of the fluctuations across the translocation step observed in the presence of Me^{2+} (26). Neither the forward nor reverse translocation displacement requires Me^{2+}. However, in the absence of Me^{2+}, the probability of occupancy of the lower amplitude, post-translocation state (p) is higher than when complexes are captured in the presence of Me^{2+} (Fig. 3). Addition of Me^{2+} to the bulk phase elicits a decrease in p for complexes formed with both DNA1-H_OH, which bears a natural 2′-H, 3′-OH primer terminus, or DNA1-H_H, which bears a 2′-H, 3′-H primer terminus (Fig. 1*C*). This is illustrated in amplitude histograms for complexes formed between the D12A/D66A mutant of Φ29 DNAP and DNA1-H_OH (Fig. 3*A*) or DNA1-H_H (Fig. 3*B*),

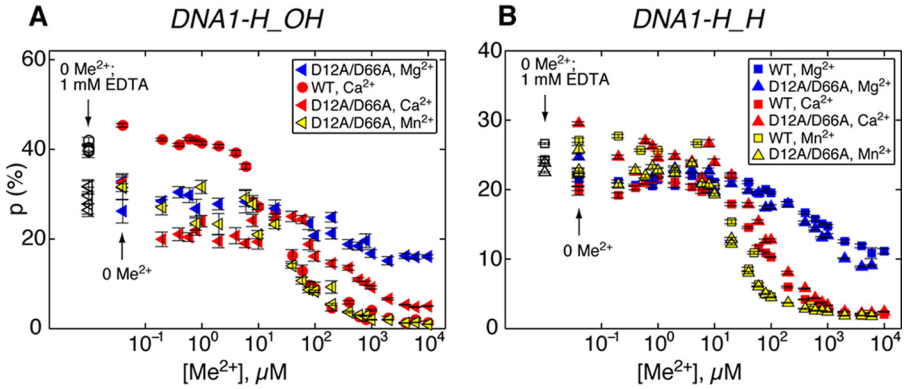

FIGURE 4. **Concentration-dependent effects of Me^{2+} on the probability of the post-translocation state.** *A*, concentration-dependent effects on *p* of Mg^{2+} (*blue symbols*), Ca^{2+} (*red symbols*), or Mn^{2+} (*yellow symbols*) for complexes formed between DNA1-H_OH and the wild type enzyme (*circles*) or the D12A/D66A enzyme (*sideways triangles*). *B*, concentration-dependent effects on *p* of Mg^{2+} (*blue symbols*), Ca^{2+} (*red symbols*), or Mn^{2+} (*yellow symbols*) for complexes formed between DNA1-H_H and the wild type enzyme (*squares*) or the D12A/D66A enzyme (*triangles*). For each plotted data point, dwell time samples at each experimental condition are extracted from 10 to 20 time traces of captured complexes. Each typical time trace comprises a segment of ~10 s, recorded at 100 kHz, and thus consisting of 1 million data points. Because there is no 0 value on the log scale horizontal axis of the plots in *A* and *B*, values for *p* determined in the absence of added Me^{2+} (from each individual titration experiment) are placed on the plots at the position for 0.04 μM Me^{2+}, and are indicated by an *arrow* and label (0 Me^{2+}). Values for equivalent complexes, captured in separate control experiments in the absence of Me^{2+} and presence of 1 mM EDTA, are placed on the plots at the position for 0.01 μM Me^{2+}. These values are indicated in *A* for complexes of DNA1-H_OH with the wild type enzyme (*open black circles*) or with the D12A/D66A enzyme (*open black sideways triangles*), and in *B* for complexes with DNA1-H_H with the wild type enzyme (*open black squares*) or the D12A/D66A enzyme (*open black triangles*), by an *arrow* and label (0 Me^{2+}; 1 mM EDTA). Within the range of experiment to experiment variation, the measured *p* values were unaffected by the presence or absence of EDTA. This indicates that Me^{2+} titration experiments, performed in the absence of EDTA, are not affected by residual or contaminating Me^{2+} in the system. Complexes in the Me^{2+} titration experiments were captured at 180 mV applied potential.

captured in either the absence of Me^{2+} (Fig. 3, *A*, *i*, and *B*, *i*) or in the presence of 6 mM Mg^{2+} (Fig. 3, *A*, *ii*, and *B*, *ii*), 6 mM Ca^{2+} (Fig. 3, *A*, *iii*, and *B*, *iii*), or 6 mM Mn^{2+} (Fig. 3, *A*, *iv*, and *B*, *iv*). The D12A/D66A mutant lacks two of the ligands for the catalytic Me^{2+} ions in the exonuclease active site and thus has negligible exonucleolytic activity (40, 41). This permits experiments to be conducted with DNA1-H_OH in the presence of Mg^{2+} or Mn^{2+}, conditions under which the 2′-H, 3′-OH terminated primer strand would be degraded in the bulk phase by the wild type enzyme (26, 35). The extent to which *p* was decreased for the D12A/D66A complexes varied with the identity of the metal species; for both DNA1-H_OH and DNA1-H_H, Mn^{2+} caused the largest decrease in *p*, followed by Ca^{2+} and then Mg^{2+} (Fig. 3).

We examined the effects of Me^{2+} concentration on the probability of the post-translocation state in Φ29 DNAP complexes by performing titration experiments spanning five orders of magnitude, from 0.2 to 10,000 μM Me^{2+}. For DNA1-H_OH, we used the wild type enzyme in Ca^{2+} titration experiments, and the D12A/D66A enzyme in titration experiments with Mg^{2+}, Ca^{2+}, and Mn^{2+} (Fig. 4*A*). Because the 2′-H, 3′-H primer terminus of DNA1-H_H inhibits the onset of Φ29 DNAP-catalyzed exonucleolytic digestion of the primer strand relative to substrates bearing 2′-H, 3′-OH termini (35), it affords protection for DNA in experiments conducted with the wild type enzyme in the presence of Mg^{2+} or Mn^{2+}. This protection permitted us to examine the effects of all three metals (Mg^{2+}, Ca^{2+}, and Mn^{2+}) on complexes formed between DNA1-H_H with the wild type enzyme and those with D12A/D66A enzyme in the titration experiments (Fig. 4*B*).

For complexes formed with DNA1-H_OH in the absence of Me^{2+}, but not those formed with DNA1-H_H in the absence of Me^{2+}, the identity of the enzyme causes a difference in *p*; for wt Φ29 DNAP at 0 Me^{2+}, $p \approx 45\%$ (Fig. 4*A*), whereas for the D12A/D66A mutant at 0 Me^{2+} $p \approx 30\%$ (Figs. 3*A*, *i*, and 4*B*). For all complexes examined, formed with either the wild type or D12A/D66A enzyme, and either the DNA1-H_OH or DNA1-H_H substrate, Me^{2+} causes a concentration-dependent decrease in *p*. For most of the complexes, the decrease in *p* occurs primarily within the concentration range of ~10 to 1000 μM Me^{2+} (Fig. 4); the exception is the response of *p* to Ca^{2+} for the complexes of the wild type enzyme with DNA1-H_OH (Fig. 4*A*). For this complex, the decrease in *p* begins at a lower concentration (between ~6 and 8 μM) than it does for D12A/D66A complexes formed with DNA1-H_OH (~10 μM). Furthermore, for the wild type complexes formed with DNA1-H_OH, *p* drops precipitously in response to Ca^{2+}, reaching a lower level than for the D12A/D66A enzyme at concentrations above ~60–80 μM. At $[Ca^{2+}] \geq$ ~1000 μM, *p* for the wild type enzyme resolves to ~1–2 and ~4–5% for the D12A/D66A enzyme.

Me^{2+} Concentration-dependent Resolution of Kinetic Complexity in the Primer Strand Transfer Pathway—We sought to determine the kinetic mechanisms that contribute to the Me^{2+}-dependent decrease in probability of post-translocation state occupancy. Although the net effect of Me^{2+} for each DNAP-DNA complex is a decrease in *p* relative to the same complex in the absence of Me^{2+}, any subset of the noncovalent transitions that govern the probability of the post-translocation state could be affected by Me^{2+} (Fig. 2*B*), and the magnitude and Me^{2+}-concentration dependence of effects on each transition could vary depending upon the identity of the partners in the DNAP-DNA complex and upon the identity of the metal. We first examined the survival probability *versus* dwell time of upper amplitude dwell time samples and that of lower amplitude dwell time samples, extracted from ionic current traces for complexes captured in the Me^{2+} titration experiments (Figs. 5 and 6). The survival probability as a function of time *t* is defined as the probability that the dwell time is larger than *t*. The observed survival probability is calculated as the fraction of dwell time samples larger than *t*.

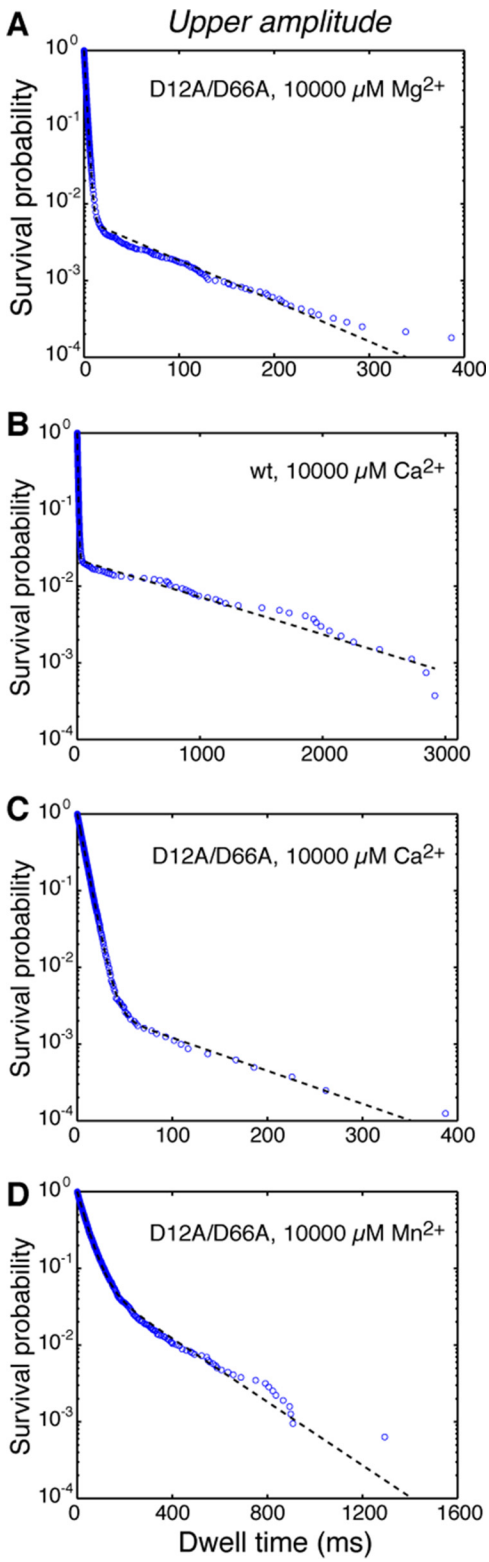

FIGURE 5. **Survival probability of the upper amplitude at 10,000 μM Me^{2+}.** Survival probability *versus* dwell time plots for dwell time samples extracted from the upper amplitude of ionic current traces, for complexes formed between DNA1-H_OH and (*A* and *C-D*) the D12A/D66A enzyme or (*B*) the wild type enzyme. Complexes were captured in the presence of 10,000 μM Mg^{2+} (*A*), 10,000 μM Ca^{2+} (*B* and *C*), or 10,000 μM Mn^{2+} (*D*). *Blue circles* represent the data points, and the *dashed black line* represents maximum likelihood estimation fitting to a model of two exponential modes.

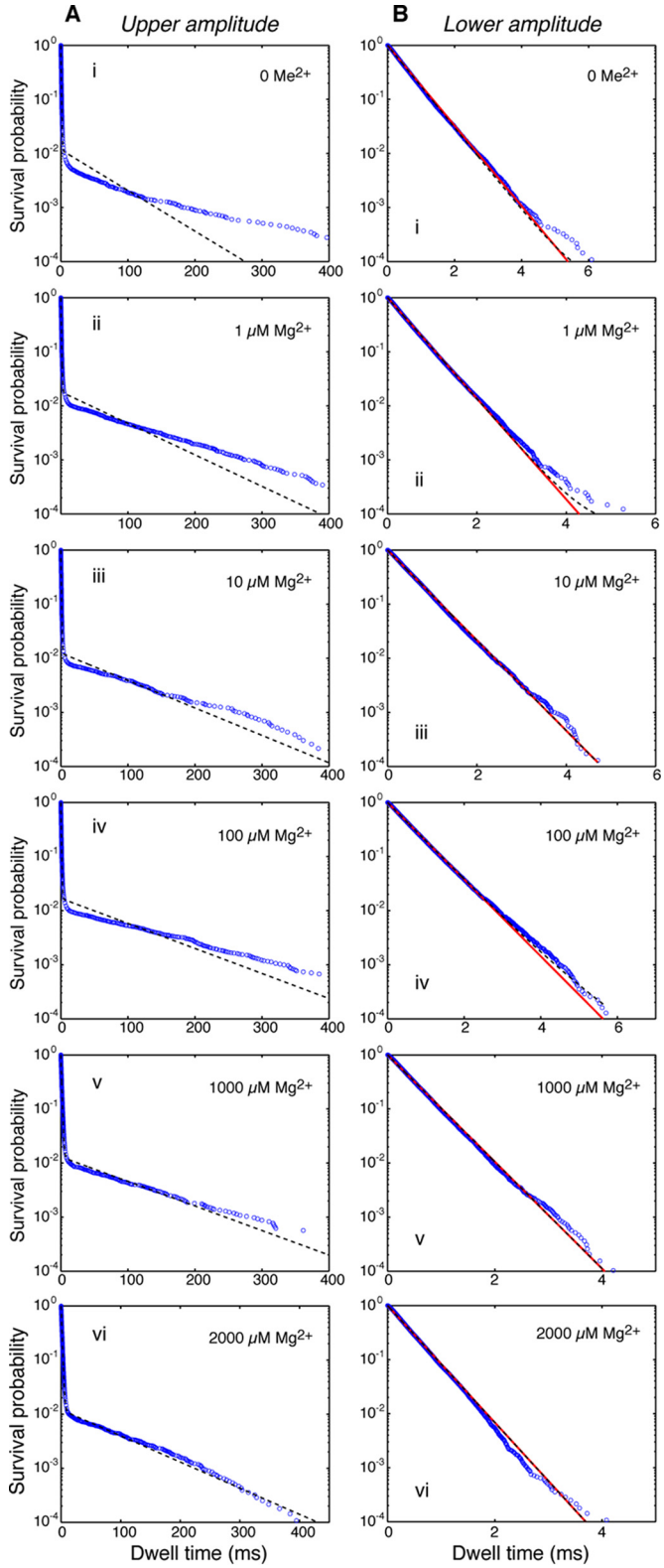

FIGURE 6. **Effects of Me^{2+} on the survival probability of each of the two amplitude levels.** Survival probability *versus* dwell time plots based on dwell time samples extracted from *A*, the upper amplitude, or *B*, the lower amplitude of ionic current traces, for complexes formed between D12A/D66A Φ29 DNAP and DNA1-H_OH. Complexes were captured in the presence of (i) 0 Me^{2+}, (ii) 1 μM Mg^{2+}, (iii) 10 μM Mg^{2+}, (iv) 100 μM Mg^{2+}, (v) 1000 μM Mg^{2+}, (vi) 2000 μM Mg^{2+}. In *A* and *B*, *blue circles* represent the data points; the *dashed black line* represents MLE (maximum likelihood estimate) fitting to a model of two exponential modes; in *B*, the *solid red line* represents maximum likelihood estimation fitting to a single exponential.

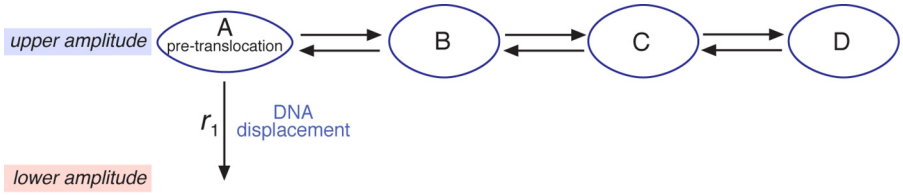

FIGURE 7. **Hypothetical kinetic diagram governing the escape from the upper amplitude.** At 0 Me^{2+} and low [Me^{2+}], the upper amplitude dwell time shows more than two exponential modes (Fig. 6), which indicates that the primer strand transfer pathway between the polymerase and exonuclease sites contains multiple kinetic states, and is no longer described by a pair of transition rates (r_3 and r_4 as in Fig. 2*B*). Even in that case, the forward translocation rate r_1 can still be reliably calculated from measured dwell time samples (see "Results").

In the presence of 10 mM Mg^{2+}, the upper amplitude survival probability for binary complexes formed between the D12A/D66A enzyme with DNA1-H_OH is well fit by a model of two exponential modes (26) (Fig. 5*A*). We have shown that these two kinetic states in the upper amplitude correspond to (i) stays of the complex in the pre-translocation state in the polymerase site, and (ii) stays of the complex in the state in which the primer strand occupies the exonuclease site (26). Upper amplitude survival probability for complexes captured in 10 mM Ca^{2+}, formed between DNA1-H_OH and either the wild type enzyme (Fig. 5*B*) or the D12A/D66A enzyme (Fig. 5*C*), are also well fit by a model of two exponential modes, as are complexes of the D12A/D66A enzyme with DNA1-H_OH captured in 10 mM Mn^{2+} (Fig. 5*D*).

However, in the absence of Me^{2+} (Fig. 6*A*, *i*), and across a wide range of [Me^{2+}] up to almost 1000 μM the distribution of upper amplitude dwell time for complexes formed with the DNA1-H_OH substrate deviates from a distribution of two exponential modes. This is illustrated in Fig. 6*A*, *i-iv*, for complexes captured in 0, 1, 10, and 100 μM Mg^{2+}. The upper amplitude survival probability contains more than two exponential modes, suggesting the possibility that at low [Me^{2+}], residence in the exonuclease site may be described by multiple kinetic states, rather than a single kinetic state. As [Mg^{2+}] is increased into the mmiilmolar range (Figs. 5*A* and 6*A*, *v* and *vi*), survival probability of the upper amplitude converges to a model of two exponential modes.

Qualitatively similar kinetic complexity (deviation from two exponential modes) at Me^{2+} concentrations below ~1000 μM was observed for the upper amplitude for all of the complexes examined in the Mg^{2+}, Ca^{2+}, or Mn^{2+} titration experiments. In addition, as we have previously reported, when complexes formed between either the wild type or D12A/D66A enzyme and the DNA1-H_H substrate are captured in the presence of high [Me^{2+}], plots of survival probability *versus* dwell time of the upper amplitude are fit by a single exponential decay function. This decay rate corresponds to the inverse of the forward translocation rate (24, 26). Thus, for the DNA1-H_H complexes at high [Me^{2+}], a population of dwell time samples that corresponds to stays of the primer strand in the exonuclease site cannot be resolved. This, combined with the kinetic complexity in the upper amplitude observed in the presence of 0 or submillimolar Me^{2+} for complexes formed with either DNA1-H_OH or DNA1-H_H, precludes our ability to reliably quantify the effects of Me^{2+} on the rates of primer strand transfer between the polymerase and exonuclease site (Fig. 2*B*, r_3 and r_4).

Despite the kinetic complexity in the upper amplitude, the effects of Me^{2+} ions on the forward and reverse rates of translocation can be reliably determined. First, for each of the complexes examined, in the absence of Me^{2+}, and across the entire range of [Me^{2+}], survival probability of the lower amplitude is well fit by a single exponential decay function (Fig. 6*B*) (24, 26); thus the reverse translocation rate (r_2) can be calculated from the data. Second, despite the complexity of the upper amplitude dwell time distribution observed at 0 Me^{2+} and at Me^{2+} concentrations below ~1000 μM (Fig. 6*A*, *i–iv*), r_1 can also be determined across the [Me^{2+}] titration series. This is illustrated using a hypothetical example for the kinetic complexity of the upper amplitude dwell time cluster (Fig. 7), in which the upper amplitude comprises four kinetic states: A, B, C, and D, where state A is the pre-translocation state. The forward translocation rate (r_1) is the rate of escaping from state A to the lower amplitude, and can be accurately determined from the measured survival probability. Let S(t) be the upper amplitude survival probability as a function of dwell time t. Mathematically, no matter how kinetically complex the upper amplitude is, it holds for Equation 5.

$$r_1 = -\left.\frac{dS(t)}{dt}\right|_{t=0} \qquad \text{(Eq. 5)}$$

That is, the forward translocation rate r_1 is the initial decay rate of the survival probability.

The Influence of Me^{2+} on Φ29 DNAP Translocation Rates—Me^{2+} ions have notable effects on both forward rate (r_1) and reverse rate (r_2) of the translocation fluctuations (Fig. 8). For all complexes examined, formed between either the wild type or D12A/D66A enzymes, with either the DNA1-H_OH or DNA1-H_H substrates, Me^{2+} causes a concentration-dependent decrease in r_1. The [Me^{2+}]-dependent decreases in r_1 (Fig. 8, *A* and *C*) largely mirror the [Me^{2+}]-dependent decreases in p (Fig. 4, *A* and *B*); the decrease in the forward translocation rate (r_1) makes the dominant contribution to the decrease in the probability of the post-translocation state (p). As with the decrease in p, the effects of Me^{2+} on r_1 occur primarily within the concentration regime of ~10 to ~1000 μM Me^{2+} (Fig. 8, *A* and *C*). Also in accord with the decrease in p, the extent to which r_1 was decreased for the D12A/D66A complexes varied with the identity of the metal species; for both DNA1-H_OH and DNA1-H_H, Mn^{2+} elicited the greatest decrease in r_1, followed by Ca^{2+} and then Mg^{2+} (Fig. 8, *A* and *C*). In complexes formed with DNA1-H_OH, the higher value of p observed in the absence of Me^{2+} for the wild type enzyme relative to the D12A/

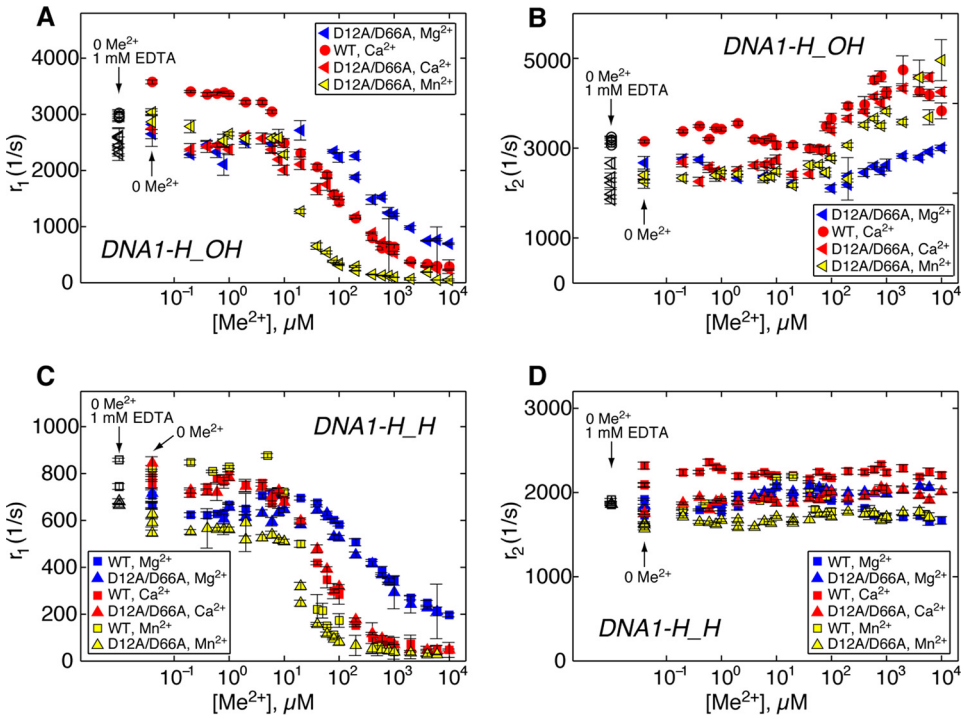

FIGURE 8. **Concentration-dependent effects of Me^{2+} on Φ29 DNAP translocation rates.** Plots of (*A* and *C*) r_1 *versus* [Me^{2+}] and (*B* and *D*) r_2 *versus* [Me^{2+}] for complexes formed with the DNA1-H_OH substrate (*A* and *B*) or with the DNA1-H_H substrate (*C* and *D*). The *shapes and colors* of symbols for the complexes in *A* and *B* are displayed in the *inset box* and are described in the legend for Fig. 4*A*; the *shapes and colors* of symbols for the complexes in *C* and *D* are displayed in the *inset box* and are described in the legend for Fig. 4*B*. Within the range of experiment to experiment variation, the values for r_1 and r_2 for each of the DNAP-DNA complexes captured in the absence of added Me^{2+} (indicated by an *arrow* and label: 0 Me^{2+}) do not vary from those of the equivalent complexes, captured in control experiments in the absence of Me^{2+} and in the presence of 1 mM EDTA (indicated by an *arrow* and label: 0 Me^{2+}; 1 mM EDTA).

D66A enzyme (Fig. 4) is also accounted for, at least in part, by a difference in r_1 for the two enzymes in the absence of Me^{2+} (Fig. 8*A*). For wild type complexes formed with DNA1-H_OH at 0 Me^{2+}, $r_1 \approx 3400$/s, whereas for D12A/D66A complexes formed with DNA1-H_OH at 0 Me^{2+}, $r_1 \approx 2700$/s. With DNA1-H_OH, the effects of Me^{2+} on complexes formed with both enzymes can only be compared for Ca^{2+}; we note that the Ca^{2+} concentration at which r_1 begins to decrease differs for the two enzymes, with the decrease in r_1 beginning at ~0.2 μM Ca^{2+} for the wild type enzyme and at ~1 μM for the D12A/D66A enzyme. At Ca^{2+} concentrations above ~1 μM, the values of r_1 for the two enzymes converge (Fig. 8*A*).

For complexes formed with either the wild type or D12A/D66A enzymes, Me^{2+} causes a concentration-dependent increase in r_2 that is dependent upon the presence of the primer terminal 3′-OH group: the increase is observed for complexes formed with DNA1-H-OH (Fig. 8*B*) but not for complexes formed with DNA1-H_H (Fig. 8*D*). The increase in r_2 is much more modest than the decrease in r_1. The Me^{2+}-dependent increase in r_2 becomes detectable at ~100 μM Me^{2+}, an order of magnitude higher than the concentration required to observe the decrease in r_1. In complexes formed with the D12A/D66A enzyme, r_2 continues to increase as a function of either Mg^{2+} or Mn^{2+} up to at least 10,000 μM, the highest concentration tested. In contrast, the ability of Ca^{2+} to cause an increase in r_2, in complexes formed with either the wild type or D12A/D66A enzymes, appeared to saturate above ~2000 μM (Fig. 8*B*). Like the decrease in r_1, the extent to which r_2 was increased for the D12A/D66A complexes varied with the identity of the metal species, but the rank order of effectiveness among the three metal ions at eliciting the increase in r_2 differs from the effect on r_1; Ca^{2+} elicited the greatest increase in r_2, followed by Mn^{2+}, and then by Mg^{2+}, which had modest effects (Fig. 8*B*).

The Relationship Among the Effects of Me^{2+}, the Identity of the Primer Terminus, and the Translocation Energy Landscape—The influence of Me^{2+} ions on the magnitude of both r_1 and r_2 uncovered in the Me^{2+} titration experiments (Fig. 8) prompted us to examine the effect of Me^{2+} ions on the energy landscape across the translocation step (Fig. 9). The Me^{2+} titration experiments were conducted by capturing Φ29 DNAP complexes at a single applied voltage (180 mV). When complexes are held atop the nanopore, the force applied by the voltage impedes the rate of the forward translocation (r_1) and increases the rate of the reverse translocation (r_2). Plots of log(r_1) *versus* voltage and log(r_2) *versus* voltage both fit to straight lines, indicating that the force is applied along the direction of the translocation (24). The Me^{2+} ions could influence both the rate at a given voltage and the dependence of the rates on voltage. The slope of log(r_1) *versus* voltage is negative and proportional to the distance between the pre-translocation state and the transition state for the translocation step; the slope of log(r_2) *versus* voltage is positive and proportional to the distance between the transition state and the post-translocation state (24).

We showed previously that the primer terminal 3′-OH group is a determinant in the energy landscape of the translocation (26). When complexes are captured at 180 mV in the presence of 10 mM Mg^{2+}, r_1 is ~3.8-fold faster in complexes with DNA1-

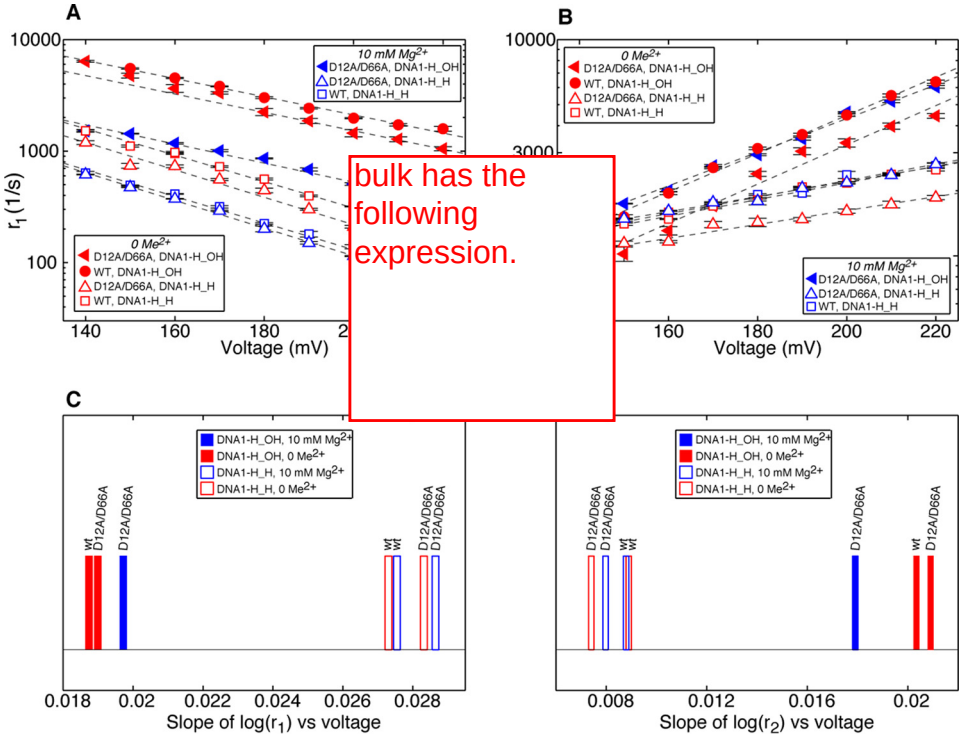

FIGURE 9. **Effects of Me^{2+} on the response of the translocation rates to applied force.** Plots of log(r_1) (*A*) *versus* voltage and log(r_2) (*B*) *versus* voltage for complexes formed between DNA1-H_OH (*filled symbols*) or DNA1-H_H (*unfilled symbols*) and either wild type Φ29 DNAP or D12A/D66A Φ29 DNAP. Complexes were captured in the presence of either 0 Me^{2+}, 1 mM EDTA (*red symbols*) or 11 mM Mg^{2+}, 1 mM EDTA (*blue symbols*). Rates were determined from dwell time samples extracted from ionic current traces and a three-state kinetic model (26) consisting of transitions r_1, r_2, r_3, and r_4 in the model diagram in Fig. 2*B*. *Errors bars* indicate the standard error. The *fitting lines* in *A* and *B* were generated by linear least squares fitting. The absolute values of the slopes of the fitting lines for each of the complexes are plotted in *C* for log(r_1) and in *D* for log(r_2).

H_OH than it is in complexes of DNA1-H_H. The 3′-OH group causes a decrease in the slope of log(r_1) *versus* voltage and an increase in the slope of log(r_2) *versus* voltage, indicating that in 10 mM Mg^{2+}, along the coordinate of the translocation displacement, the transition state is closer to the pre-translocation state for complexes formed with DNA1-H_OH than it is for complexes formed with DNA1-H_H (26). Because the increase in r_2 observed at high [Me^{2+}] in the Me^{2+} titration experiments is dependent upon the presence of the primer terminal 3′-OH group (Fig. 8, *B* and *D*), it was of particular interest to compare the effects of Me^{2+} ions on the energy landscape between complexes formed with DNA1-H_OH and complexes formed with DNA1-H_H. Is the influence of the 3′-OH group on the energy landscape of the translocation affected by the presence of Me^{2+}? Does the influence of the 3′-OH group in the translocation depend upon an interaction between the primer terminus and a Me^{2+} ion (or ions), or is it an inherent property of the interaction of the DNA substrate with the enzyme?

We examined the influence of Me^{2+} on the response of the translocation rates to applied force by comparing complexes captured at 0 Me^{2+} to those captured at 10 mM Mg^{2+}, across the range of voltages from 140 to 220 mV (Fig. 9). Experiments were conducted in the absence of Me^{2+} with both the wild type and the D12A/D66A enzymes, for complexes formed with both DNA1-H_OH and DNA1-H_H; in 10 mM Mg^{2+} with both enzymes for complexes formed with DNA1-H_H; and in 10 mM Mg^{2+} with the D12A/D66A enzyme for complexes formed with DNA1-H_OH. The higher values for r_1 in the absence of Me^{2+} relative to values for r_1 in 10 mM Me^{2+} that were observed in the Me^{2+} titration experiments conducted at 180 mV (Fig. 8, *A* and *C*) hold across the voltage range examined, for complexes formed with either DNA-H_OH or DNA1-H_H (Fig. 9*A*). In addition, as previously observed for complexes captured in the presence of 10 mM Mg^{2+}, in the absence of Me^{2+}, r_1 is faster in complexes formed with DNA1-H_OH than it is for complexes formed with DNA1-H_H. For complexes formed with DNA1-H_OH, there is a modest decrease in the slope of log(r_1) *versus* voltage relative to that for complexes formed with DNA1-H_H, in the absence of Me^{2+} or in the presence of 10 mM Mg^{2+} (Fig. 9*A*). The 3′-OH group exerts an effect on the slope of log(r_2) *versus* voltage that is more substantial in relative magnitude to its effect on the slope of log(r_1) *versus* voltage. In complexes with DNA1-H_OH, the slope of log(r_2) *versus* voltage is increased relative to that for complexes formed with DNA1-H_H, in the presence of 10 mM Mg^{2+} or the absence of Me^{2+} (Fig. 9*B*).

We compared the absolute values of the slopes of the fitting lines in the log(rate) *versus* voltage plots (Fig. 9, *C* and *D*). The slope values for log(r_1) *versus* voltage as well as those for log(r_2) *versus* voltage show two discrete clusters. For r_1, a cluster for complexes formed with DNA1-H_OH is centered at ~0.019, and a cluster for complexes formed with DNA1-H_H is centered at ~0.028 (Fig. 9*C*). In the case of r_2, a cluster for complexes formed with DNA1-H_OH is centered at ~0.02, and a cluster for complexes formed with DNA1-H_H is centered at ~0.008 (Fig. 9*D*). For both log(r_1) *versus* voltage and log(r_2) *versus* voltage, the dependence of slope on force is a function of

the primer terminus identity, regardless of the presence or absence of Me^{2+}.

The Influence of Me^{2+} on Complementary dNTP Binding—Me^{2+} ions are essential for both dNTP binding and catalysis in the polymerase active site. The identity of the Me^{2+} ions bound in the polymerase active site can strongly influence dNTP binding affinity and binding rates (33), as well as the fidelity of dNTP selection and the ability to catalyze phosphodiester bond formation (see Refs. 10, 42, and 43 and references therein). Because the forward translocation fluctuation precedes dNTP binding, dNTP binds to complexes only when they are in the post-translocation state (Fig. 2*B*) (25). In the nanopore assay the two translocation states are fully resolved and the effects of dNTP on the equilibrium between the two translocation states can be quantified. Furthermore, because dNTP stabilizes the lower amplitude, post-translocation state (Fig. 2*A*, *ii*) by extracting and analyzing dwell time samples in a stochastic model, the rates of dNTP binding to and dissociating from the post-translocation state can be quantified (25).

We compared the binding affinity for dGTP (complementary to dCMP at $n = 0$ of DNA1 in Fig. 1*C*) and dGTP binding rates, in complexes formed with D12A/D66A enzyme, captured in the presence of 10 mM Mg^{2+}, Mn^{2+}, or Ca^{2+} (Fig. 10; Table 1).

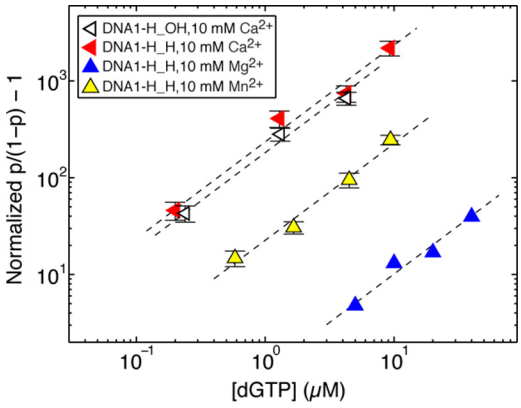

FIGURE 10. **Complementary dNTP binding affinity compared as a function of Me^{2+} species and primer terminus identity.** Complexes were formed between the D12A/D66A mutant of Φ29 DNAP and DNA1-H-OH in 10 mM Ca^{2+} (*black unfilled sideways triangles*), or with DNA1-H_H in 10 mM Ca^{2+} (*red filled triangles*), 10 mM Mg^{2+} (*blue filled triangles*), or 10 mM Mn^{2+} (*yellow filled triangles*). The binding affinity is examined using the log-log plot of (normalized $p/(1-p) - 1$) *versus* dGTP concentration. We have shown that the vertical intercept of the log-log plot at [dGTP] = 1 μM is given by -log(K_d) (23). The higher the log-log plot is vertically, the smaller the value of K_d and the stronger the binding affinity. *Error bars* show the standard errors.

For Ca^{2+}, we conducted dGTP titration experiments with both DNA1-H_OH and DNA1-H_H; for Mg^{2+} and Mn^{2+}, we used DNA1-H_H in dGTP titration experiments. The affinity for dNTP among different DNAP-DNA complexes can be directly compared by plotting the normalized $p/(1-p)$, where p is the probability of post-translocation state occupancy. The normalized $p/(1-p)$ is defined as the value of $p/(1-p)$ in the presence of a given concentration of dNTP, divided by the value of $p/(1-p)$ for the same complex captured in the absence of dNTP (in the presence of Me^{2+} of the same identity and concentration). The normalized $p/(1-p)$ is independent of the transitions between the two translocation states in the absence of dNTP (23, 32), which vary among the complexes and conditions compared. In addition, we have shown that (normalized $p/(1-p) - 1$) = [dNTP]/K_d, where [dNTP] is the concentration of dNTP (23). This theoretical expression predicts that the log-log plot of (normalized $p/(1-p) - 1$) *versus* [dNTP] is a straight line with slope = 1 and vertical intercept = -log(K_d) at [dNTP] = 1 μM. Thus K_d is determined from the vertical intercept at [dNTP] = 1 μM, obtained in fitting observed data points to the theoretical expression. A higher vertical position in the log-log plot of (normalized $p/(1-p) - 1$) *versus* [dNTP] corresponds to a smaller value for K_d and a stronger binding affinity (Fig. 10; Table 1).

For D12A/D66A complexes formed with DNA1-H_H in Mg^{2+}, the dNTP binding affinity is $K_d \approx 1$ μM (in Mg^{2+}) (Table 1) (33). Both Mn^{2+} and Ca^{2+} cause an enhancement in dNTP binding affinity compared with complexes captured in Mg^{2+}, with Mn^{2+} yielding a decrease in the value of K_d by ~25-fold, to $K_d \approx 0.04$ μM (in Mn^{2+}), and Ca^{2+} decreasing the value of K_d more significantly, by an additional order of magnitude to $K_d \approx 0.004$ μM (in Ca^{2+}). The stronger affinity afforded in Mn^{2+} relative to Mg^{2+} is primarily due to an ~18-fold decrease in the dNTP dissociation rate, in good accord with an earlier comparison between dNTP binding parameters for the D12A/D66A mutant captured in 10 mM Mg^{2+} or in 2 mM Mn^{2+} (33). The more substantial enhancement in dNTP binding affinity for complexes captured in Ca^{2+} occurs due to a combination of an ~9-fold increase in the dNTP association rate constant and an ~23-fold decrease in the dNTP dissociation rate, relative to the binding rates for complexes captured in Mg^{2+}. Because Ca^{2+} supports dNTP binding but does not support phosphodiester bond formation, this afforded an opportunity to examine the effect of the primer terminal 3′-OH group, a ligand for metal A (15), on dNTP binding by comparing complexes formed with

TABLE 1

Complementary dNTP binding rates in complexes formed with the D12A/D66A mutant of Φ29 DNAP

Rates were determined using dwell time samples extracted from ionic current traces (see "Experimental Procedures") and a three-state kinetic model (consisting of transitions r_1, r_2, k_{on}, and k_{off} in the model diagram in Fig. 1*A*). Complexes were captured at 180 mV in the presence of 1 mM EDTA, with 11 mM $MgCl_2$, or 11 mM $CaCl_2$, or 11 mM $MnCl_2$ as indicated; K_d, k_{on}[dNTP], and k_{off} are independent of the applied voltage (23, 25). All values are reported with the standard error.

DNA	Me^{2+}	k_{on} [a]	k_{off} [b]	k_{off}/k_{on}	K_d [c]
		$s^{-1}\mu M^{-1}$	s^{-1}	$s^{-1}/s^{-1}\mu M^{-1}$	μM
DNA1-H_OH	Ca^{2+}	147.67 ± 14.75	0.767 ± 0.085	0.0052 ± 0.0006	0.00551 ± 0.0005
DNA1-H_H	Ca^{2+}	150.19 ± 13.85	0.624 ± 0.082	0.0043 ± 0.0007	0.00426 ± 0.0005
DNA1-H_H	Mg^{2+}	16.7 ± 0.4	17.7 ± 0.3	1.02 ± 0.02	0.988 ± 0.091
DNA1-H_H	Mn^{2+}	21.85 ± 2.81	0.978 ± 0.13	0.0448 ± 0.0067	0.0444 ± 0.0036

[a] The dNTP association rate constant.
[b] The dNTP dissociation rate.
[c] K_d values for the binding of dGTP to the post-translocation state are determined from the vertical intercepts of the fitting lines to the log-log plot of (normalized $p/(1-p) - 1$) *versus* [dGTP], where p is equilibrium probability of the lower amplitude level (see the model diagram in Fig. 2*B*). The plot of (normalized $p/(1-p) - 1$) *versus* [dGTP] is shown in Fig. 10.

DNA1-H_OH or with DNA1-H_H. The presence or absence of the primer terminal 3′-OH group does not significantly affect the ground state dNTP binding parameters (Fig. 10; Table 1); k_{on}, k_{off}, and K_d are each very similar for complexes formed with both DNA substrates.

Discussion

In this study, we hypothesized that because the divalent cations (Me^{2+} ions) that are essential for catalytic function in both the polymerase and exonuclease active sites of replicative DNAPs serve as intimate components of the architecture in each of the sites, they may exert significant influence on the noncovalent transitions that occur in DNAP-DNA complexes during each nucleotide addition cycle. To test this, we applied a nanopore-based, single molecule approach that features single-nucleotide spatial precision and sub-millisecond temporal resolution to determine the effects of Mg^{2+}, Ca^{2+}, and Mn^{2+} on the kinetic transitions of translocation, dNTP binding, and primer strand transfer between the polymerase and exonuclease active sites (Fig. 2*B*), in individual complexes formed with Φ29 DNAP, a B-family replicative DNAP.

Me^{2+} Ions Alter the Equilibrium Across the Translocation Step, and the Forward and Reverse Translocation Rates—Fluctuations across the translocation step, during which the DNAP moves with respect to its DNA substrate by the distance of a single nucleotide, occur in the absence of Me^{2+}, indicating that the translocation fluctuations are an activity inherent to the DNAP-DNA complex. Nonetheless, Me^{2+} ions have a significant influence on the translocation. For all Φ29 DNAP-DNA complexes examined, formed with either the wild type or D12A/D66A enzyme, and either the DNA1-H_OH or DNA1-H_H substrate, Me^{2+} causes a concentration-dependent decrease in the probability of the post-translocation state (p) (Fig. 4). This shift in equilibrium is promoted by Mg^{2+} and Mn^{2+}, which support DNAP catalysis, and Ca^{2+}, which supports dNTP binding but not catalysis. It is caused primarily by a [Me^{2+}]-dependent decrease in the forward translocation rate (r_1) (Fig. 8, *A* and *C*). The Me^{2+}-dependent decrease in r_1 may be attributable to stabilization of the fingers-closed pre-translocation state, which would be predicted to slow the forward translocation (3). The pre-translocation state that is sampled during the nanopore experiments corresponds to the product of the covalent addition of the primer terminal residue during DNA synthesis, after pyrophosphate has dissociated from the complex (presumably complexed with the metal B ion) (26, 35). Although we cannot assign whether the Me^{2+}-dependent decrease in r_1 is caused by binding of Me^{2+} at the metal A or metal B site, the Me^{2+}-dependent effects on the escape from the pre-translocation state suggest that while the environment of both metal binding sites necessarily changes significantly after catalysis, at least one of the sites retains affinity for Me^{2+}.

Each of the three metals examined also promoted a modest concentration-dependent increase in the backward transition rate from the post-translocation to pre-translocation state (r_2) that is dependent upon the presence of a 3′-OH group at the primer terminus of the DNA substrate (Fig. 8, *B* and *D*). The dependence of the increase in r_2 on the primer strand 3′-OH implicates this group as a ligand for the metal ion that elicits the increase, suggesting that it is the post-translocation state metal A ion and implying that the metal A ion binds to the Φ29 DNAP-DNA complexes independent of the presence of dNTP. In complexes formed with a DNA substrate bearing a 3′-H primer terminus, where the increase in r_2 is not observed (Fig. 8*D*), we cannot distinguish between the case in which metal A does not bind, or the case in which it binds but does not cause an increase in r_2.

In the nanopore experiments, the applied voltage exerts a force on the captured DNAP-DNA complex along the direction of the translocation. Although Me^{2+} modulates the translocation rates at a given applied force (Fig. 8), it does not alter the dependence of the rates on force, for complexes formed with either DNA1-H_OH or with DNA1-H_H (Fig. 9). The primer terminal 3′-OH group is a determinant in the energy landscape of the translocation (26); its presence alters the slopes of both log(r_1) *versus* voltage and log(r_2) *versus* voltage. When complexes captured at 0 Me^{2+} are compared with those captured at 10 mM Mg^{2+}, across a range of applied voltages from 140 to 220 mV (Fig. 9, *A* and *B*), the dependence of the slopes of both log(r_1) *versus* voltage and log(r_2) *versus* voltage are observed to be a function of the primer terminus identity, regardless of the presence or absence of Me^{2+} (Fig. 9, *C* and *D*). The smaller slope of log(r_1) *versus* voltage and larger slope of log(r_2) *versus* voltage for complexes formed with DNA1-H_OH relative to complexes formed with DNA1-H_H indicates that the transition state for the translocation is closer to the pre-translocation state when the DNA substrate bears a primer terminal 3′-OH group than when the DNA substrate bears a primer terminal 3′-H group, independent of the presence or absence of Me^{2+}. Thus, Me^{2+} affects the translocation rates at each given voltage, but not the dependence of the rates on force, indicating that Me^{2+} does not perturb the translocation distances among the pre-translocation state well, the post-translocation state well, and the transition state, which are strongly influenced by the primer terminal 3′-OH group. Like the translocation fluctuations, the influence of the primer terminal 3′-OH on the energy landscape of the translocation is inherent to the DNAP-DNA complex.

Me^{2+} Ion Identity Affects Complementary dNTP Binding Equilibrium and Rates—Complementary dNTP binding in the post-translocation state polymerase active site is strongly affected by Me^{2+} identity, with Ca^{2+} affording the highest affinity, followed by Mn^{2+}, and then Mg^{2+} (Fig. 10; Table 1). Both Ca^{2+} and Mn^{2+} substantially decrease the dNTP dissociation rate relative to Mg^{2+}; Ca^{2+} also yields an increase in the dNTP association rate constant. In contrast to Mn^{2+} and Mg^{2+}, Ca^{2+} does not support phosphodiester bond formation, yielding the opportunity to examine the effect of the primer terminal 3′-OH group, which is a ligand for metal A (15), on dNTP binding. Somewhat surprisingly, the presence or absence of the primer terminal 3′-OH group does not significantly affect the ground state dNTP binding parameters (Fig. 10; Table 1), which are very similar for complexes formed with DNA1-H_OH or DNA1-H_H. This indicates that the presence or absence of the primer terminal 3′-OH group is not a determinant for ground state dNTP binding in Ca^{2+}.

Because selective stabilization of the transition state over the ground state contributes to catalytic efficiency and specificity (44), it is possible that the enhanced ground state stabilization effected by both Mn^{2+} and Ca^{2+} contributes to the effects of these metals on phosphodiester bond formation. Because k_{off} reflects the free energy difference between the dNTP-bound post-translocation state and the dNTP-unbound post-translocation state, the smaller values of k_{off} for complexes formed in Mn^{2+} or Ca^{2+} relative to complexes formed in Mg^{2+} may obtain, at least in part, from a deeper free energy well for the dNTP-bound ground state. In addition to affecting the free energy difference between the dNTP-bound and unbound states, a deeper free energy well could affect the free energy difference between the dNTP-bound ground state and the transition state for catalysis. Among the three metals we examined, the largest stabilization of ground state dNTP binding is caused by Ca^{2+}, and this metal does not support catalytic function. Ground state stabilization by Mn^{2+}, while an order of magnitude more modest than Ca^{2+}, is almost 20-fold greater than that afforded by Mg^{2+}; while Mn^{2+} supports catalysis, it is at a cost to fidelity in nucleotide selection.

The relationship among Me^{2+} ions, dNTP binding, and conformational transitions associated with dNTP binding has been studied for pol β (45), for the Klenow fragment of DNA polymerase I (an A-family repair DNAP) (46), and for the B-family replicative DNAP from bacteriophage RB69 (47, 48). Not surprisingly, details vary among these enzymes, which have different functional roles and are from different DNAP families. Nonetheless, the studies are consistent with a general scenario in which metal B is sufficient to support dNTP binding and the associated fingers-closing conformational change, whereas both metals A and B are required for phosphodiester bond formation.

The effects of Me^{2+} ions on dNTP binding or on the translocation that we have measured in Φ29 DNAP-DNA complexes may be related, at least in part, to Me^{2+}-dependent effects on the rates of fingers opening and closing. Based on earlier findings that both r_1 and k_{off} are slower for complexes captured in 2 mM Mn^{2+} than for complexes captured in 10 mM Mg^{2+}, we had hypothesized that Mn^{2+} may exert its effects on both r_1 and k_{off} by decreasing the rate of fingers opening from the closed complex (33). This hypothesis is based upon the structural model proposed for translocation (3), which predicts that decreasing the rate of fingers opening in the pre-translocation state would lead to a decrease in the rate of the forward translocation (r_1). Similarly, because it is reasonable to assume that dNTP dissociation requires fingers opening, a decrease in the rate of fingers opening could yield a decrease in the dissociation rate of dNTP (k_{off}) from the dNTP-bound post-translocation state. The findings in the current study that both r_1 and k_{off} are lower in Ca^{2+} (Fig. 8; Table 1) than they are in Mg^{2+} provides further evidence supporting the hypothesis.

Complex Effects of Me^{2+} on the Primer Strand Transfer Pathway between the Polymerase and Exonuclease Active Sites—We previously established the correspondence between a second kinetic state in the upper amplitude and the primer strand transfer between the polymerase and exonuclease sites (26). In the current study, we examined the effects of Me^{2+} ions on primer strand transfer by applying approaches developed in the prior study, which revealed that the primer strand pathway displays significant Me^{2+}-concentration dependent kinetic complexity. In the absence of Me^{2+}, or when the [Me^{2+}] is low, the pathway for primer strand transfer between the polymerase and exonuclease sites displays more than two kinetic states (Fig. 6*A*). For complexes formed with DNA1-H_OH, this complexity resolves to two states (the pre-translocation state in the polymerase site, and the state in which the primer has been transferred to the exonuclease site) when the [Me^{2+}] is above ~1 mM (Figs. 5 and 6*A*) (26). For complexes formed with DNA1-H_H captured in the presence of high [Me^{2+}], dwell time samples that correspond to stays of the primer strand in the exonuclease site cannot be resolved from the dwell time samples that decay at a single exponential rate that corresponds to the inverse of the forward translocation rate (24, 26). Although these observed effects of [Me^{2+}] are intriguing, we are not yet able to speculate about the mechanisms governing the effects of Me^{2+} on the kinetics of the primer strand transfer pathway. Detailed dissection of the effects of [Me^{2+}] on this pathway will require biochemical and mathematical models significantly more complex than the four-state model shown in Fig. 2*B*, which we will pursue in future studies.

Finally, it is not yet known how generally applicable our findings regarding the effects of Me^{2+} ions on translocation, dNTP binding, or primer strand transfer with the Φ29 DNAP will be to other DNAPs, in large part because most techniques that have been employed to examine DNAPs cannot resolve and quantify the translocation step and the kinetic transitions that it coordinates with both single nucleotide precision and sub-millisecond temporal resolution. However, given the structural and functional conservation of the polymerase and exonuclease active sites in the B-family replicative DNAPs, it is reasonable to expect that these effects will apply to other enzymes in this family. This includes the eukaryotic nuclear leading strand and lagging strand replicative DNAPs, pol ϵ and pol δ, respectively (18, 19). In light of the finding that Me^{2+}, which stabilizes the pre-translocation state in Φ29 DNAP-DNA complexes (Fig. 8, *A* and *C*), can also stabilize the pre-translocation state in DNAP-DNA complexes of the X-family mammalian repair DNAP, pol β (22), it is also possible that our findings will extend more broadly to other DNAP families.

Author Contributions—J. M. D., K. R. L., and H. W. designed the study and wrote the paper. J. M. D. performed nanopore experiments. J. M. D., K. R. L., and H. W. analyzed the results and approved the final version of the manuscript.

Acknowledgment—We are grateful to Mark Akeson for helpful discussion and support.

References

1. Kunkel, T. A. (2009) Evolving views of DNA replication (in)fidelity. *Cold Spring Harb. Symp. Quant. Biol.* **74,** 91–101
2. Johansson, E., and Dixon, N. (2013) Replicative DNA polymerases. *Cold Spring Harbor Perspect. Biol.* **5**, a012799
3. Berman, A. J., Kamtekar, S., Goodman, J. L., Lázaro, J. M., de Vega, M., Blanco, L., Salas, M., and Steitz, T. A. (2007) Structures of ϕ29 DNA polymerase complexed with substrate: the mechanism of translocation in

B-family polymerases. *EMBO J.* **26,** 3494–3505
4. Doublié, S., Tabor, S., Long, A. M., Richardson, C. C., and Ellenberger, T. (1998) Crystal structure of a bacteriophage T7 DNA replication complex at 2.2-Å resolution. *Nature* **391,** 251–258
5. Eom, S. H., Wang, J., and Steitz, T. A. (1996) Structure of Taq polymerase with DNA at the polymerase active site. *Nature* **382,** 278–281
6. Kamtekar, S., Berman, A. J., Wang, J., Lázaro, J. M., de Vega, M., Blanco, L., Salas, M., and Steitz, T. A. (2004) Insights into strand displacement and processivity from the crystal structure of the protein-primed DNA polymerase of bacteriophage ϕ29. *Mol. Cell* **16,** 609–618
7. Wang, J., Sattar, A. K., Wang, C. C., Karam, J. D., Konigsberg, W. H., and Steitz, T. A. (1997) Crystal structure of a pol α family replication DNA polymerase from bacteriophage RB69. *Cell* **89,** 1087–1099
8. Swan, M. K., Johnson, R. E., Prakash, L., Prakash, S., and Aggarwal, A. K. (2009) Structural basis of high-fidelity DNA synthesis by yeast DNA polymerase δ. *Nat. Struct. Mol. Biol.* **16,** 979–986
9. Hogg, M., Osterman, P., Bylund, G. O., Ganai, R. A., Lundström, E.-B., Sauer-Eriksson, A. E., and Johansson, E. (2014) Structural basis for processive DNA synthesis by yeast DNA polymerase ϵ. *Nat. Struct. Mol. Biol.* **21,** 49–55
10. Yang, W., Lee, J. Y., and Nowotny, M. (2006) Making and breaking nucleic acids: two-Mg^{2+}-ion catalysis and substrate specificity. *Mol. Cell* **22,** 5–13
11. Steitz, T. A., and Steitz, J. A. (1993) A general two-metal-ion mechanism for catalytic RNA. *Proc. Natl. Acad. Sci. U.S.A.* **90,** 6498–6502
12. Beese, L. S., and Steitz, T. A. (1991) Structural basis for the 3′-5′ exonuclease activity of Escherichia coli DNA polymerase I: a two metal ion mechanism. *EMBO J.* **10,** 25–33
13. Steitz, T. A. (1993) DNA-dependent and RNA-dependent DNA polymerases. *Curr. Opin. Struct. Biol.* **3,** 31–38
14. Johnson, S. J., Taylor, J. S., and Beese, L. S. (2003) Processive DNA synthesis observed in a polymerase crystal suggests a mechanism for the prevention of frameshift mutations. *Proc. Natl. Acad. Sci. U.S.A.* **100,** 3895–3900
15. Franklin, M. C., Wang, J., and Steitz, T. A. (2001) Structure of the replicating complex of a pol α family DNA polymerase. *Cell* **105,** 657–667
16. Pelletier, H., Sawaya, M. R., Kumar, A., Wilson, S. H., and Kraut, J. (1994) Structures of ternary complexes of rat DNA polymerase β, a DNA template-primer, and ddCTP. *Science* **264,** 1891–1903
17. Batra, V. K., Beard, W. A., Shock, D. D., Krahn, J. M., Pedersen, L. C., and Wilson, S. H. (2006) Magnesium-induced assembly of a complete DNA polymerase catalytic complex. *Structure* **14,** 757–766
18. Pursell, Z. F., Isoz, I., Lundström, E.-B., Johansson, E., and Kunkel, T. A. (2007) Yeast DNA polymerase epsilon participates in leading-strand DNA replication. *Science* **317,** 127–130
19. Miyabe, I., Kunkel, T. A., and Carr, A. M. (2011) The major roles of DNA polymerases ϵ and δ at the eukaryotic replication fork are evolutionarily conserved. *PLoS Genet.* **7,** e1002407
20. Wang, M., Xia, S., Blaha, G., Steitz, T. A., Konigsberg, W. H., and Wang, J. (2011) Insights into base selectivity from the 1.8-Å resolution structure of an RB69 DNA polymerase ternary complex. *Biochemistry* **50,** 581–590
21. Johansson, E., and Macneill, S. A. (2010) The eukaryotic replicative DNA polymerases take shape. *Trends Biochem. Sci.* **35,** 339–347
22. Kirby, T. W., DeRose, E. F., Cavanaugh, N. A., Beard, W. A., Shock, D. D., Mueller, G. A., Wilson, S. H., and London, R. E. (2012) Metal-induced DNA translocation leads to DNA polymerase conformational activation. *Nucleic Acids Res.* **40,** 2974–2983
23. Dahl, J. M., Mai, A. H., Cherf, G. M., Jetha, N. N., Garalde, D. R., Marziali, A., Akeson, M., Wang, H., and Lieberman, K. R. (2012) Direct observation of translocation in individual DNA polymerase complexes. *J. Biol. Chem.* **287,** 13407–13421
24. Lieberman, K. R., Dahl, J. M., Mai, A. H., Akeson, M., and Wang, H. (2012) Dynamics of the translocation step measured in individual DNA polymerase complexes. *J. Am. Chem. Soc.* **134,** 18816–18823
25. Lieberman, K. R., Dahl, J. M., Mai, A. H., Cox, A., Akeson, M., and Wang, H. (2013) Kinetic mechanism of translocation and dNTP binding in individual DNA polymerase complexes. *J. Am. Chem. Soc.* **135,** 9149–9155
26. Lieberman, K. R., Dahl, J. M., and Wang, H. (2014) Kinetic mechanism at the branchpoint between the DNA synthesis and editing pathways in individual DNA polymerase complexes. *J. Am. Chem. Soc.* **136,** 7117–7131
27. Morin, J. A., Cao, F. J., Lázaro, J. M., Arias-Gonzalez, J. R., Valpuesta, J. M., Carrascosa, J. L., Salas, M., and Ibarra, B. (2012) Active DNA unwinding dynamics during processive DNA replication. *Proc. Natl. Acad. Sci. U.S.A.* **109,** 8115–8120
28. Blanco, L., Bernad, A., Lázaro, J. M., Martín, G., Garmendia, C., and Salas, M. (1989) Highly efficient DNA synthesis by the phage ϕ29 DNA polymerase: symmetrical mode of DNA replication. *J. Biol. Chem.* **264,** 8935–8940
29. Blanco, L., and Salas, M. (1996) Relating structure to function in ϕ29 DNA polymerase. *J. Biol. Chem.* **271,** 8509–8512
30. Salas, M., Blanco, L., Lázaro, J. M., and de Vega, M. (2008) The bacteriophage ϕ29 DNA polymerase. *IUBMB Life* **60,** 82–85
31. de Vega, M., Blanco, L., and Salas, M. (1999) Processive proofreading and the spatial relationship between polymerase and exonuclease active sites of bacteriophage ϕ29 DNA polymerase. *J. Mol. Biol.* **292,** 39–51
32. Dahl, J. M., Wang, H., Lázaro, J. M., Salas, M., and Lieberman, K. R. (2014) Kinetic mechanisms governing stable ribonucleotide incorporation in individual DNA polymerase complexes. *Biochemistry* **53,** 8061–8076
33. Dahl, J. M., Wang, H., Lázaro, J. M., Salas, M., and Lieberman, K. R. (2014) Dynamics of translocation and substrate binding in individual complexes formed with active site mutants of ϕ29 DNA polymerase. *J. Biol. Chem.* **289,** 6350–6361
34. Esteban, J. A., Bernad, A., Salas, M., and Blanco, L. (1992) Metal activation of synthetic and degradative activities of ϕ29 DNA polymerase, a model enzyme for protein-primed DNA replication. *Biochemistry* **31,** 350–359
35. Lieberman, K. R., Cherf, G. M., Doody, M. J., Olasagasti, F., Kolodji, Y., and Akeson, M. (2010) Processive replication of single DNA molecules in a nanopore catalyzed by ϕ29 DNA polymerase. *J. Am. Chem. Soc.* **132,** 17961–17972
36. Benner, S., Chen, R. J., Wilson, N. A., Abu-Shumays, R., Hurt, N., Lieberman, K. R., Deamer, D. W., Dunbar, W. B., and Akeson, M. (2007) Sequence-specific detection of individual DNA polymerase complexes in real time using a nanopore. *Nat. Nanotechnol.* **2,** 718–724
37. Akeson, M., Branton, D., Kasianowicz, J. J., Brandin, E., and Deamer, D. W. (1999) Microsecond time-scale discrimination among polycytidylic acid, polyadenylic acid, and polyuridylic acid as homopolymers or as segments within single RNA molecules. *Biophys. J.* **77,** 3227–3233
38. Garalde, D. R., Simon, C. A., Dahl, J. M., Wang, H., Akeson, M., and Lieberman, K. R. (2011) Distinct complexes of DNA polymerase I (Klenow fragment) for base and sugar discrimination during nucleotide substrate selection. *J. Biol. Chem.* **286,** 14480–14492
39. Cherf, G. M., Lieberman, K. R., Rashid, H., Lam, C. E., Karplus, K., and Akeson, M. (2012) Automated forward and reverse ratcheting of DNA in a nanopore at 5-Å precision. *Nat. Biotechnol.* **30,** 344–348
40. Bernad, A., Blanco, L., Lázaro, J. M., Martín, G., and Salas, M. (1989) A conserved 3′-5′ exonuclease active site in prokaryotic and eukaryotic DNA polymerases. *Cell* **59,** 219–228
41. Garmendia, C., Bernad, A., Esteban, J. A., Blanco, L., and Salas, M. (1992) The bacteriophage ϕ29 DNA polymerase, a proofreading enzyme. *J. Biol. Chem.* **267,** 2594–2599
42. Esteban, J. A., Salas, M., and Blanco, L. (1993) Fidelity of ϕ29 DNA polymerase: comparison between protein-primed initiation and DNA polymerization. *J. Biol. Chem.* **268,** 2719–2726
43. Johnson, K. A. (2010) The kinetic and chemical mechanism of high-fidelity DNA polymerases. *Biochim. Biophys. Acta* **1804,** 1041–1048
44. Fersht, A. (1985) *Enzyme Structure and Mechanism*, Second Ed., W.H. Freeman, New York
45. Bakhtina, M., Lee, S., Wang, Y., Dunlap, C., Lamarche, B., and Tsai, M.-D. (2005) Use of viscogens, dNTPαS, and rhodium(III) as probes in stopped-

flow experiments to obtain new evidence for the mechanism of catalysis by DNA polymerase β. *Biochemistry* **44,** 5177–5187

46. Bermek, O., Grindley, N. D., and Joyce, C. M. (2011) Distinct roles of the active-site Mg^{2+} ligands, Asp^{882} and Asp^{705}, of DNA polymerase I (Klenow fragment) during the prechemistry conformational transitions. *J. Biol. Chem.* **286,** 3755–3766
47. Wang, M., Lee, H. R., and Konigsberg, W. (2009) Effect of A and B metal ion site occupancy on conformational changes in an RB69 DNA polymerase ternary complex. *Biochemistry* **48,** 2075–2086
48. Lee, H. R., Wang, M., and Konigsberg, W. (2009) The reopening rate of the fingers domain is a determinant of base selectivity for RB69 DNA polymerase. *Biochemistry* **48,** 2087–2098